LETTER

doi:10.1038/nature24465

Haze heats Pluto's atmosphere yet explains its cold temperature

Xi Zhang[1], Darrell F. Strobel[2] & Hiroshi Imanaka[3,4]

Pluto's atmosphere is cold and hazy[1–3]. Recent observations[1] have shown it to be much colder than predicted theoretically[4], suggesting an unknown cooling mechanism[1]. Atmospheric gas molecules, particularly water vapour, have been proposed as a coolant; however, because Pluto's thermal structure is expected to be in radiative–conductive equilibrium[4–9], the required water vapour would need to be supersaturated by many orders of magnitude under thermodynamic equilibrium conditions[9]. Here we report that atmospheric hazes, rather than gases, can explain Pluto's temperature profile. We find that haze particles have substantially larger solar heating and thermal cooling rates than gas molecules, dominating the atmospheric radiative balance from the ground to an altitude of 700 kilometres, above which heat conduction maintains an isothermal atmosphere. We conclude that Pluto's atmosphere is unique among Solar System planetary atmospheres, as its radiative energy equilibrium is controlled primarily by haze particles instead of gas molecules. We predict that Pluto is therefore several orders of magnitude brighter at mid-infrared wavelengths than previously thought—a brightness that could be detected by future telescopes.

Hydrocarbon hazes have substantial radiative heating and cooling effects in planetary atmospheres, as observed for Saturn's moon Titan[10] and for Jupiter's stratosphere[11]. Globally extensive haze layers have been seen in images of Pluto taken from the New Horizons spacecraft[3]; the solar occultation observed by New Horizons' Alice ultraviolet spectrograph[2] also revealed the extinction of light by haze from the ground to at least 350 km above. Pluto's high-altitude haze particles are expected to be monomers (or macromolecules) with sizes of tens of nanometres, produced by ion chemistry and photochemistry in the presence of hydrocarbons and nitrogen[1–3] in processes similar to those observed in Titan's ionosphere[12]. Haze-formation and -transport models show that the monomers are produced at least 500 km above the ground[13,14], and possibly as high as 1,000 km (ref. 3). The monomers settle down and start to grow through coagulation and condensation at around 350 km, eventually forming fractal aggregates composed of hundreds to thousands of monomers with a fractal dimension of two, similar to Titan's haze particles[1–3]. From images taken by the LORRI instrument on board New Horizons[3], the aggregated particle size is estimated to be about 0.15 μm at 45 km. But in the near-surface region, the particle properties are not well determined[3].

Using the observed distributions of particles[3] and temperature[1,2] (Fig. 1), the radiative effects of hazes on Pluto can be quantified through a multi-scattering radiative-transfer calculation (see Methods). Given the distribution of haze from the surface to 350 km that is inferred from the Alice ultraviolet occultation[1,2], we assume that the haze ultraviolet extinction decays exponentially with the geopotential height from the ground to 700 km, where nitrogen ionization peaks and monomers are expected to form in Pluto's atmosphere[2] (Extended Data Fig. 1). The corresponding pressure level (10^{-5} Pa) on Titan occurs at about 1,100 km, where the monomers are produced and were detected by the Cassini spacecraft[12]. The optical depth of the haze at other wavelengths can be scaled from the observed ultraviolet optical depth on the basis of the extinction efficiency (Extended Data Fig. 2). In the near-surface layers, Pluto's hazes have been assumed to be composed of organic

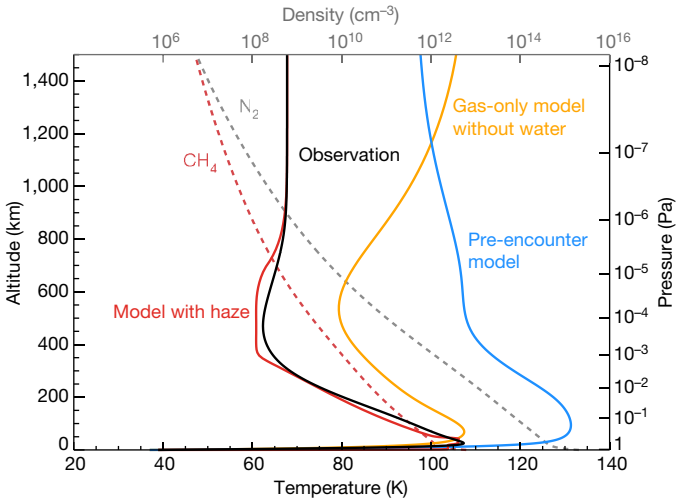

Figure 1 | Atmospheric temperature and gas-density profiles of Pluto. Dashed lines represent the densities of nitrogen (N_2) and methane (CH_4) (in number of molecules per cm^3)[1]. Carbon monoxide (CO; not shown) is well mixed in the atmosphere, with a volume mixing ratio of 5×10^{-4}. Solid lines show the actual temperature profile derived by the New Horizons spacecraft (black line)[1], as well as profiles calculated using the New Horizons pre-encounter model (pale blue line)[4] and the latest gas-only model (yellow line)[9]; the latter includes hydrogen cyanide (HCN) and acetylene (C_2H_2) but not water. The red curve shows the temperature modelled herein, which includes haze-mediated heating and cooling. The key differences in the actual observed atmosphere compared with the pre-encounter predictions[4] were a compact atmosphere rather than an extended atmosphere, and an isothermal upper atmosphere rather than one indicative of escaping, adiabatically cooled atmosphere. This discrepancy implies an important but still unknown cooling process in Pluto's atmosphere[1]. HCN and C_2H_2 have been suggested as missing coolants[1,29]. But even taking into account the radiative effects of supersaturated HCN, as constrained by recent Atacama Large Millimeter/submillimetre Array (ALMA) observations[29], the predicted quasi-isothermal temperature is still about 100 K (see figure 7a of ref. 8), in comparison with the observed temperature of 70 K. Including the non-local thermodynamic equilibrium cooling process from the C_2H_2 ν_5 band does reduce the temperature down from a peak value of about 107 K at 25 km (yellow line), but not enough to achieve the broad minimum observed temperature of about 63 K at 400 km (black line)[9]. Water vapour was proposed as the last possible gaseous cooling candidate after the other possibilities were rejected, but the required abundance would be implausibly supersaturated by many orders of magnitude[9].

[1]Department of Earth and Planetary Sciences, University of California Santa Cruz, Santa Cruz, California 95064, USA. [2]Department of Earth & Planetary Sciences and Physics & Astronomy, Johns Hopkins University, Baltimore, Maryland 21218, USA. [3]SETI Institute, 189 North Bernardo Avenue, Suite 100, Mountain View, California 94043, USA. [4]NASA Ames Research Center, Moffett Field, California 94035, USA.

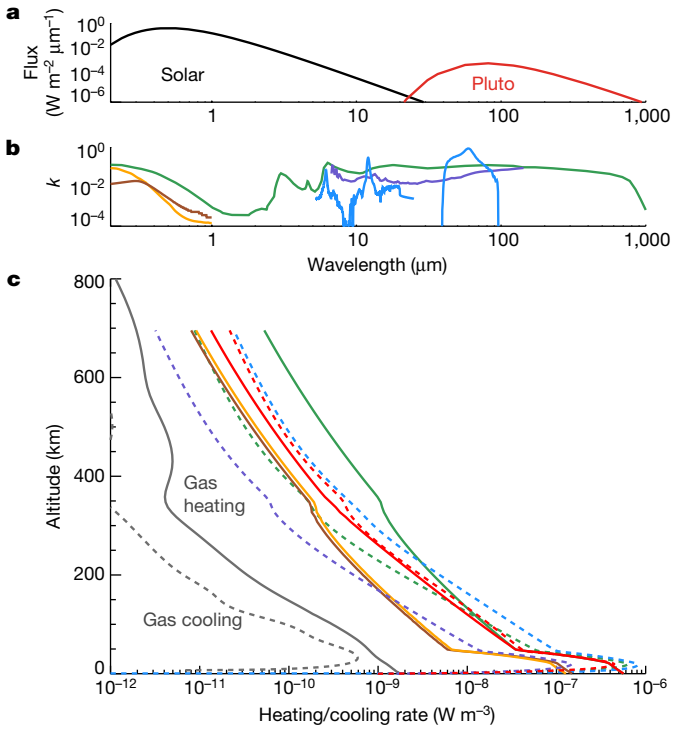

Figure 2 | Radiative heating and cooling in the atmosphere of Pluto. **a**, Globally averaged solar flux received by Pluto (black line), approximated by a blackbody of 5,778 K, and Pluto's surface emission flux (red line), approximated by a blackbody of 38.9 K. **b**, Imaginary part of the particle refractive indices (k) from various sources (yellow line, ref. 15; green line, ref. 17; brown line, ref. 19; dark blue line, ref. 20; pale blue lines, ref. 30 (for amorphous HCN ice)). **c**, Profiles showing rates of radiative heating (solid lines) and cooling (dashed lines), based on the observed temperature profile (Fig. 1). Colours are as in **b**; in addition, the red lines show a radiative equilibrium case (balanced model) with altitude-dependent k values (Extended Data Fig. 1d) bounded by laboratory measurements[15,16]. The balanced model yields the haze model temperature profile shown in Fig. 1. The gas-only heating rate from CH_4 (solid grey line) is much larger than the gas-cooling rate from CO, HCN and C_2H_2 (dashed grey line; see Methods)[9]. We calculated the haze heating and cooling rates (coloured lines) using the particle distributions in Extended Data Fig. 1 and the k values in **b** to illustrate the uncertainty range.

materials similar to Titan's tholins[1–3]. However, the optical properties of Pluto's haze materials could be different to those of Titan's haze. Previous laboratory measurements of the plausible haze composition demonstrated large variations in haze optical constants, reflecting distinct formation chemistry and different chemical structures[15,16]. Here we explore different refractive indices to test the uncertainty range of the heating and cooling rates in Pluto's atmosphere (Fig. 2). In the ultraviolet and visible heating regime, the imaginary part of the refractive index (k) could vary by more than an order of magnitude[17–19]. In the infrared cooling regime we use laboratory tholin measurements[17], as well as empirically derived k values from Titan that are based on Cassini observations at the 100 Pa level[20].

We find that hazes on Pluto have substantial solar heating and infrared cooling rates (Fig. 2c). This is expected, because the retrieved vertical extinction optical depth of particles is of the order of 0.1 in ultraviolet and 0.01 in visible wavelengths, on the basis of Alice ultraviolet spectrograph and LORRI observations, respectively[1–3]. Given Pluto's globally averaged solar flux of about 300 mW m^{-2} (Fig. 2a) and its surface albedo of 0.8 (ref. 21), the absorbed solar flux by particles in the ultraviolet and visible range must be greater than 1 mW m^{-2}. We investigated multiple solutions of fractal aggregates that fit the reflectivity observations from LORRI (Extended Data Fig. 3), as well as the possibility that the near-surface particles are mostly aggregates (Extended Data Fig. 4)[2]. Our sensitivity studies show that the uncertainties associated with these factors are smaller than the uncertainties resulting from the large variations in optical constants. Nevertheless, the haze heating and cooling rates in all cases are consistently larger than the gas heating and cooling rates by one to two orders of magnitude (Fig. 2). Below 700 km, the vertically integrated heating rate due to haze ranges from 3 mW m^{-2} to 17 mW m^{-2}, and the cooling rate from 4 mW m^{-2} to 20 mW m^{-2}. In the same altitude range, the integrated heating rate caused by methane (CH_4) is only around 0.1 mW m^{-2}, and the infrared cooling rate due to carbon monoxide (CO), hydrogen cyanide (HCN) and acetylene (C_2H_2) is about 0.03 mW m^{-2}. Consequently, the total radiative energy budget in the atmosphere must be dominated by haze particles instead of gas molecules.

The haze-mediated heating and cooling rates can be balanced within the uncertainty range to yield the derived temperature profile (Fig. 1). In the lower 50 km, the haze heating can be approximately balanced by the cooling by using the haze optical constants from ref. 17 (Fig. 2). In the upper region, the heating and cooling profiles are not precisely balanced at each pressure level unless we invoke altitude-dependent k values (Extended Data Fig. 2). On Titan, k values of hazes have also been found (from Cassini-Huygens observations) to vary with altitude[22]. On Pluto, once the aggregates have formed at about 350 km, supersaturated HCN and C_2 hydrocarbons start to condense onto the monomers[13,23]. HCN ice particles have also been observed in Titan's stratosphere[24]. The haze cooling rate from pure HCN ices might be larger than the cooling rate resulting from the organic tholins (Fig. 2). Once the organic haze particles are coated by HCN and hydrocarbon ices, their optical properties (that is, the effective k values) as well as their heating and cooling rates are likely to be altered with altitude. Although the uncertainty of optical properties is large, there are solutions for achieving the atmospheric energy balance on Pluto (Fig. 2). As an example, we demonstrate here one possible solution—a radiative 'balanced model' with altitude-dependent k values bounded by laboratory measurements[15,16]. A similar modification of the laboratory k values was also required in models to maintain the thermal energy balance in Titan's atmosphere[25]. With the optimized refractive indices in the balanced model, a level-by-level atmospheric radiative equilibrium is achieved between the solar heating

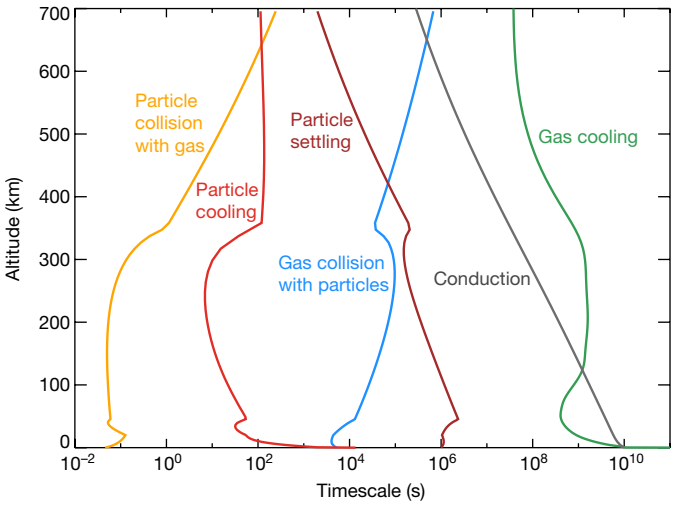

Figure 3 | Heat-transfer timescales in the atmosphere of Pluto. The particle (or gas) heat-transfer timescale resulting from gas–particle collisions (yellow and blue lines) is shorter than the particle (or gas) radiative cooling timescale (red and green lines) at all altitudes below 700 km, implying that gas and particles should be in thermal equilibrium. The radiative relaxation (cooling) timescale of the haze particles (red line) is around a few minutes, shorter than the particle-settling timescale (brown line). Heat conduction (grey line) dominates the heat transfer in the gas phase at altitudes higher than 700 km.

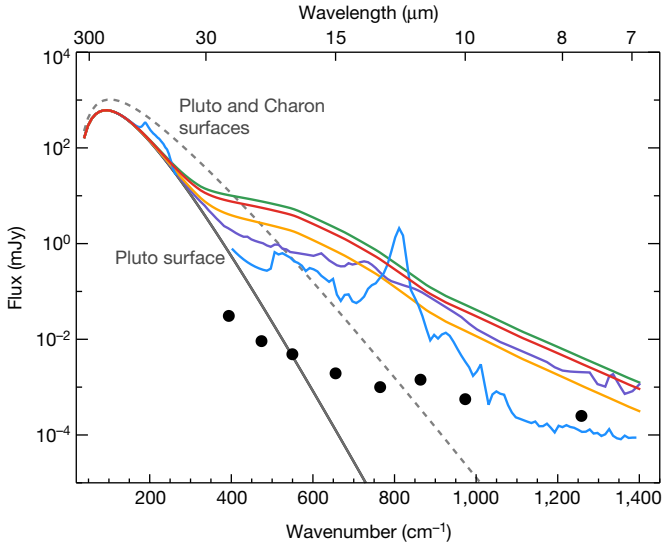

Figure 4 | Infrared spectra of Pluto with flux values at Earth's distance, with and without the effects of haze radiation from Pluto's atmosphere. The dots indicate the 10σ faint-source detection limits in a 10,000-s integration for several channels of the Mid-Infrared Instrument imager on the James Webb Space Telescope[28]. The coloured spectra are based on several models of haze-mediated cooling, as in Fig. 2 (green line, ref. 17; dark blue line, ref. 20; pale blue line, ref. 30; red line, our balanced model). The yellow line corresponds to a model in which the near-surface haze layers are composed of fractal aggregates instead of Mie particles[17] (Extended Data Fig. 4). If Pluto's atmosphere were cooled by supersaturated water vapour instead of haze particles, then low-resolution (for example, 0.1 cm^{-1}) spectra would seem to be similar to Pluto's surface blackbody (solid grey line) or to the combined Pluto and Charon surface spectrum (dashed grey line), because the narrow water rotational lines are averaged out at low resolution.

and infrared cooling—including both gas and haze—below 700 km (Fig. 2).

Efficient heat transfer maintains thermal equilibrium between gas and haze particles through collisions below 700 km. The mean free path of a particle in Pluto's thin atmosphere is more than 1,000 μm—much greater than the submicrometre particle size. The haze particle must thus be located in the free-molecule regime[13], within which heat transfer between the gas and particle phases is controlled by collisions. The collisional timescale is much shorter than the radiative relaxation timescale in each phase (Fig. 3; see Methods). The radiative relaxation timescale of the haze particles is also shorter than the particle-settling timescale. Therefore, the thermal energy of the gas and haze particles below 700 km should quickly reach equilibrium owing to collisions before any other heat-transfer processes take place. If there is any net radiative heating from the gases, then the excess energy will be transferred rapidly to the haze particles and radiated away, leading to a decrease of the gas temperature. Owing to strong radiative cooling from the hazes, the radiative timescale of the entire atmosphere below 700 km is probably of the order of months to a few Earth years—shorter than the cooling timescale resulting from gas alone (about ten Earth years). Above 700 km, because the thermal conduction timescale in the gas phase decreases continuously with altitude, conduction must dominate the gas-mediated heat transfer, having a greater effect than gas–particle collisions and gas radiative relaxation. The gas-mediated temperature in the upper atmosphere is thus primarily controlled by conduction, even if the haze particles extend to 1,000 km. Our radiative–conductive calculation shows that the gas temperature is in equilibrium with the haze temperature below 700 km, above which thermal conduction maintains a nearly isothermal atmosphere. The calculated gas temperature profile is consistent with the New Horizons observations (Fig. 1).

Interestingly, methane on Neptune's moon Triton is much less abundant than on Pluto and Titan, and is photochemically destroyed in the lower atmosphere, leading to a much lower rate of formation of haze particles, which concentrate only at low altitudes[26]. Consequently, haze on Triton has a much smaller cooling effect, resulting in a warmer upper atmosphere than on Pluto[9]. A strong haze-mediated cooling in the infrared on Pluto will result in a large radiation flux to space. Conventionally, Pluto has been assumed to have a blackbody spectrum in terms of its surface temperature. However, on the basis of the haze-mediated radiation, we predict that Pluto should appear several orders of magnitude brighter than its surface blackbody spectrum would imply at wavelengths shorter than 25 μm (Fig. 4). Even taking into account contamination from the warm emission of its moon Charon, Pluto's haze radiation still exhibits a strong infrared excess at wavelengths shorter than 15 μm. The Spitzer space telescope[27] observed the total flux from the Pluto–Charon system only at wavelengths longer than 20 μm, and therefore could not distinguish Pluto's haze radiation from Charon's flux. However, the Mid-Infrared Instrument imager[28] on the James Webb Space Telescope should be able to detect the haze-induced infrared excess on Pluto, and distinguish between the effects of haze versus cooling by water rotational lines (Fig. 4).

Online Content Methods, along with any additional Extended Data display items and Source Data, are available in the online version of the paper; references unique to these sections appear only in the online paper.

Received 23 July; accepted 27 September 2017.

1. Gladstone, G. R. *et al.* The atmosphere of Pluto as observed by New Horizons. *Science* **351,** aad8866 (2016).
2. Young, L. A. *et al.* Structure and composition of Pluto's atmosphere from the New Horizons solar ultraviolet occultation. *Icarus* **300,** 174–199 (2017).
3. Cheng, A. F. *et al.* Haze in Pluto's atmosphere. *Icarus* **290,** 112–133 (2017).
4. Zhu, X. *et al.* The density and thermal structure of Pluto's atmosphere and associated escape processes and rates. *Icarus* **228,** 301–314 (2014).
5. Yelle, R. V. & Lunine, J. I. Evidence for a molecule heavier than methane in the atmosphere of Pluto. *Nature* **339,** 288–290 (1989).
6. Hubbard, W. B. Nonisothermal Pluto atmosphere models. *Icarus* **84,** 1–11 (1990).
7. Lellouch, E. Pluto's atmospheric structure: clear vs hazy models. *Icarus* **108,** 255–264 (1994).
8. Strobel, D. F. *et al.* On the vertical thermal structure of Pluto's atmosphere. *Icarus* **120,** 266–289 (1996).
9. Strobel, D. F. & Zhu, X. Comparative planetary nitrogen atmospheres: density and thermal structures of Pluto and Triton. *Icarus* **291,** 55–64 (2017).
10. Tomasko, M. G. Heat balance in Titan's atmosphere. *Planet. Space Sci.* **56,** 648–659 (2008).
11. Zhang, X. *et al.* Aerosol influence on energy balance of the middle atmosphere of Jupiter. *Nat. Commun.* **6,** 10231 (2015).
12. Lavvas, P. *et al.* Aerosol growth in Titan's ionosphere. *Proc. Natl Acad. Sci. USA* **110,** 2729–2734 (2013).
13. Gao, P. *et al.* Constraints on the microphysics of Pluto's photochemical haze from New Horizons observations. *Icarus* **287,** 116–123 (2017).
14. Bertrand, T. & Forget, F. 3D modeling of organic haze in Pluto's atmosphere. *Icarus* **287,** 72–86 (2017).
15. Imanaka, H. *et al.* Laboratory experiments of Titan tholin formed in cold plasma at various pressures: implications for nitrogen-containing polycyclic aromatic compounds in Titan haze. *Icarus* **168,** 344–366 (2004).
16. West, R. *et al.* in *Titan: Surface, Atmosphere and Magnetosphere* (eds Mueller-Wodarg, I. *et al.*) 285–321 (Cambridge Univ. Press, 2014).
17. Khare, B. N. *et al.* Optical constants of organic tholins produced in a simulated titanian atmosphere: from soft X-ray to microwave frequencies. *Icarus* **60,** 127–137 (1984).
18. Lavvas, P. *et al.* The detached haze layer in Titan's mesosphere. *Icarus* **201,** 626–633 (2009).
19. Ramirez, S. I. *et al.* Complex refractive index of Titan's aerosol analogues in the 200–900 nm domain. *Icarus* **156,** 515–529 (2002).
20. Vinatier, S. *et al.* Optical constants of Titan's stratospheric aerosols in the 70–1500 cm^{-1} spectral range constrained by Cassini/CIRS observations. *Icarus* **219,** 5–12 (2012).
21. Buratti, B. J. *et al.* Global albedos of Pluto and Charon from LORRI New Horizons observations. *Icarus* **287,** 207–217 (2017).
22. Tomasko, M. G. *et al.* A model of Titan's aerosols based on measurements made inside the atmosphere. *Planet. Space Sci.* **56,** 669–707 (2008).
23. Wong, M. L. *et al.* The photochemistry of Pluto's atmosphere as illuminated by New Horizons. *Icarus* **287,** 110–115 (2017).
24. Anderson, C. M. & Samuelson, R. E. Titan's aerosol and stratospheric ice opacities between 18 and 500 μm: vertical and spectral characteristics from Cassini CIRS. *Icarus* **212,** 762–778 (2011).

25. McKay, C. P., Pollack, J. B. & Courtin, R. The thermal structure of Titan's atmosphere. *Icarus* **80,** 23–53 (1989).
26. Herbert, F. & Sandel, B. R. CH_4 and haze in Triton's lower atmosphere. *J. Geophys. Res. Space Phys.* **96,** 19241–19252 (1991).
27. Lellouch, E. *et al.* Thermal properties of Pluto's and Charon's surfaces from Spitzer observations. *Icarus* **214,** 701–716 (2011).
28. Glasse, A. *et al.* The Mid-Infrared Instrument for the James Webb Space Telescope, IX: predicted sensitivity. *Publ. Astron. Soc. Pacif.* **127,** 686–695 (2015).
29. Lellouch, E. *et al.* Detection of CO and HCN in Pluto's atmosphere with ALMA. *Icarus* **286,** 289–307 (2017).
30. Moore, M. H. *et al.* Infrared spectra and optical constants of nitrile ices relevant to Titan's atmosphere. *Astrophys. J. Suppl. Ser.* **191,** 96–112 (2010).

Acknowledgements We thank Y. Yung, B. Bézard, E. Lellouch, M. Liang, X. Zhu and P. Gao for discussions. X.Z. acknowledges partial support from NASA Solar System Workings grant NNX16AG08G. D.F.S. acknowledges partial support from NASA's New Horizons Mission. H.I. acknowledges support from NASA Cassini Data Analysis grant NNX14AF61G and NASA Exoplanet Research grant NNX15AQ73G.

Author Contributions X.Z. conceived the research, performed the calculations and wrote the manuscript. D.F.S. provided the New Horizons data and the gas-only model and assisted with analysis. H.I. provided the refractive indices of haze particles. D.F.S. and H.I. contributed to manuscript writing.

Author Information Reprints and permissions information is available at www.nature.com/reprints. The authors declare no competing financial interests. Readers are welcome to comment on the online version of the paper. Publisher's note: Springer Nature remains neutral with regard to jurisdictional claims in published maps and institutional affiliations. Correspondence and requests for materials should be addressed to X.Z. (xiz@ucsc.edu).

Reviewer Information *Nature* thanks R. West and Y. Yung for their contribution to the peer review of this work.

METHODS

Model description. Hydrodynamic escape is not expected from Pluto's cold atmosphere[1]. Our one-dimensional model assumes that the entire atmosphere is still hydrostatic[4] and spherically symmetrical[2], with thermal escape (Jeans escape) processes occurring at the exobase. The governing equation follows the radiative–conductive heat-transport equation[4–9], but here we include both gas and particle phases:

$$(c_{p,p}\rho_p + c_{p,g}\rho_g)\frac{\partial T}{\partial t} = \frac{1}{r}\frac{\partial}{\partial r}\left(r^2 K_c \frac{\partial T}{\partial r}\right) + R_{net} + R_{adb} \quad (1)$$

where r is the radial distance from Pluto's centre; T is temperature; and $c_{p,g}$ and $c_{p,p}$ are the specific heat at a constant pressure of gas or particle, respectively. ρ_g and ρ_p are the mass density of the gas and particle, respectively; because most of the atmospheric mass is in the gas phase, $c_{p,p}\rho_p \ll c_{p,g}\rho_g$. The thermal conductivity, K_c, for the N_2–CH_4–CO gas[6] is $K_c = K_0 T^{\alpha}$, where $\alpha = 1.12$; $K_0 = 5.63$ erg cm^{-1} s^{-1} K$^{-2.12}$. $R_{net} = R_{net,g} + R_{net,p}$ is the net radiative heating rate including both gas ($R_{net,g}$) and haze ($R_{net,p}$) contributions, but $R_{net,p}$ applies only to altitudes below 700 km. R_{adb} is the adiabatic cooling rate resulting from atmospheric expansion as N_2 and CH_4 escape from the top of the atmosphere[4,31]. We assumed that the gas and particles are in thermal equilibrium below 700 km (Fig. 3). We neglect the heat transfer owing to particle settling, because the settling timescale is much longer than the haze radiative timescale (Fig. 3).

We use a semi-implicit scheme (the Crank–Nicolson scheme) to solve the system. The vertical discretization follows a non-uniform grid from previous radiative–conductive models of Pluto[4,9]. We assume an isothermal atmosphere at the upper boundary, that is, zero thermal conductive flux consistent with the slow thermal escape of N_2 and CH_4. The surface temperature is set to 38.9 K on the basis of the New Horizons observations[32]. Because the gas and particle phases are in thermal equilibrium, we do not need to solve for the particle phase explicitly. This allows us to use a longer numerical time step (typically 10^4–10^5 s) for equation (1) than the particle radiative timescale (Fig. 3). We evolve the system until the model reaches steady state. We also tested different initial conditions to ensure that all cases converge to the same final solution. The gas-only version of this model has been validated against the latest radiative–conductive models of Pluto[4,9].

Radiative heating and cooling from gases. The gas radiation is not important here because its radiative effect is much smaller than the effect of haze radiation. Our scheme basically follows the published gas-only radiative–conductive model[9]. We include the radiative heating effects of CH_4 in the extreme-ultraviolet, far-ultraviolet and near-infrared bands at 2.3 μm, 3.3 μm and 7.6 μm, respectively. The infrared CH_4 heating is in non-local thermodynamic equilibrium (non-LTE). For 7.6 μm, we solved the solar heating and infrared cooling equations together. For the gas radiative cooling, we used the radiative-transfer model initially developed for Jupiter[11,33]. We include the rotational lines of CO and HCN and the C_2H_2 vibrational–rotational band in the thermal infrared[10]. For the spectral information of gases, we used the HITRAN 2012 database[34]. We set the spectral grid to be finer than 0.00005 cm^{-1} in order to resolve the rotational line shape owing to Doppler broadening, and we treated the gas opacity using the correlated-k method[8]. We used a two-layer model[33] to calculate the non-LTE cooling rate from the C_2H_2 vibrational–rotational band at 13.7 μm. We normalized the deactivation rate of C_2H_2 in a nitrogen environment to the value in ref. 35 with CH_4 ν_4 band temperature dependence: $k_{C_2H_2-N_2} = 2.43 \times 10^{-14}\exp((T-240)/105)$ cm^3 s^{-1}, with an Einstein coefficient of 5.1 s^{-1}. The cooling effect of C_2H_6 is negligible.

The abundances of N_2, CH_4, and C_2H_2 were obtained from New Horizons observations[1,2]. The HCN abundances are from ALMA observations[29]. CO is well mixed in the atmosphere, with a volume mixing ratio of 5×10^{-4}. The vertical profiles of the major gases N_2 and CH_4 are shown in Fig. 1. Heating and cooling rates from individual gases and spectral bands can be found in Fig. 6 of ref. 9.

Radiative heating and cooling from hazes. We calculated the haze-mediated heating and cooling rates by using a multi-scattering radiative-transfer model that was initially developed to analyse Jupiter's atmosphere[11]. We assumed that the particles are produced as 10-nm monomers at 700 km. We also performed a sensitivity study on monomer size (Extended Data Figs 3, 4). According to one haze-formation model[13], the particles start growing as aggregates at altitudes of 350 km or below. The mean volume-equivalent particle radius of an aggregated particle increases in an approximately linear trend with decreasing altitude, finally reaching 0.15 μm at 45 km (ref. 3 and Extended Data Fig. 1a). The particles in the near-surface layers are assumed to be spherical[3], but we also tested a scenario involving fractal aggregates (Extended Data Fig. 4). The spherical particle size is assumed to be in a log-normal distribution[3], with an effective radius (r_{eff}) of 0.5 μm and an effective variance (v_{eff}) of 0.02. The Alice ultraviolet observations show that the ultraviolet-attenuation factor of haze particles decays exponentially with altitude from the ground to 350 km; this exponential decay can be extrapolated to 700 km under the assumption that the haze density is approximately proportional to the N_2 density (Extended Data Fig. 1b)[2]. On the basis of the observed haze attenuation factor at about 185 nm, we can derive the particle number-density profile (Extended Data Fig. 1c), subject to the constraints provided by the cross-section of the far-ultraviolet extinction. The shape of the derived number-density profile looks similar to the results obtained from a microphysical model of Titan (see Fig. 4 in ref. 36).

The imaginary parts of the refractive indices (k) from different sources are shown in Fig. 2. For the ultraviolet and visible range, using the optical constants from ref. 17 gives the upper bound of the heating rate, while using refs 15 and 19 yields a lower bound. At the infrared wavelengths, the k values are derived from Cassini observations[20], which incorporate the far-infrared data[24] but do not cover the wavenumber range between 10 cm^{-1} and 70 cm^{-1}; thus we adopt the values from ref. 17, the only available laboratory measurement in that spectral range. For low-temperature amorphous HCN ices, we use the available laboratory experiments[30] at 75 K at wavelengths between 100 cm^{-1} and 280 cm^{-1}, and between 400 cm^{-1} and 1,450 cm^{-1}.

The extinction cross-sections, single scattering albedos and phase functions of spherical particles are calculated on the basis of a Mie-sphere code[37]. For aggregated particles with a fractal dimension of two, we used a fractal aggregates code developed previously for Titan's haze[22]. The total vertical optical depth, extinction efficiency and single scattering albedo for a monomer particle and fractal aggregates are shown in Extended Data Fig. 2. On the basis of the observed haze optical depth[2] at about 185 nm, we scaled the optical depth of the haze particles at other wavelengths from the far-ultraviolet optical depth, by using the ratio of the extinction efficiency at other wavelengths to that at far-ultraviolet wavelengths (Extended Data Fig. 2a).

In order to achieve a radiative energy balance for haze particles, we used altitude-dependent k values for solar heating and cooling in our proposed 'balanced model'. The scaling factors are shown in Extended Data Fig. 1d. The k values in the ultraviolet and visible wavelengths (0.2–1 μm)[17] decrease linearly from unity at 45 km to 0.25 at 350 km, and remain constant with 0.25 scaling factor to 700 km. The k values in the infrared[17] are increased by a factor of 2.5 above 350 km, and the scaling factor varies linearly with altitude from 0.7 at 45 km and stays constant below that altitude. As noted, the adjustment to the k values is well within the uncertainty range of the laboratory measurements[15,16].

For the solar heating calculation in the ultraviolet and visible wavelengths, from 0.2 μm to 1 μm, we carried out multiple scattering calculations using 32 streams. Using 64 streams does not alter the heating rates. We used a globally averaged surface albedo of 0.8 (ref. 21). For the thermal cooling calculation, we treated the particles as pure absorbers from 10 cm^{-1} to 1,450 cm^{-1}, because their single scattering albedo is very low (Extended Data Fig. 2c) and no scattering calculation is needed.

In addition to testing different values of optical constants for hazes in Fig. 2, we also tested different choices of aggregates. We found that multiple solutions could explain the phase dependence of the reflectivity (I/F, where I is the reflected intensity and πF is the radiant flux) observed by LORRI at 45 km (ref. 3). Using the optical constants from ref. 18, we tested aggregates with: first, 10-nm monomers and an equivalent radius of 0.15 μm; second, 30-nm monomers and an equivalent radius of 0.42 μm; and third, 50-nm monomers and equivalent radius of 0.45 μm. Simulated phase functions were scaled to fit the observations (Extended Data Fig. 3). We computed the heating and cooling rates from these possible choices (Extended Data Fig. 4). Generally, the difference is within a factor of two to three—less than the uncertainty associated with the optical constants (Fig. 2).

The properties of particles in the near-surface region are not well determined[3]. The modelled aggregate particles produce a backscattered intensity that is smaller than that observed by LORRI by a factor of about three[3]. It has been argued that supersaturated hydrocarbons and nitriles rapidly condense onto the fractal particles, rendering them spherical particles of 0.5 μm. However, spherical particles do not fit with the Alice ultraviolet solar occultation data[3]. Here we tested two possible scenarios. If we use aggregates when modelling altitudes below 45 km, then the heating and cooling rates are lower by an order of magnitude than if we use spherical particles (Extended Data Fig. 4). But this reduction in rates is still smaller than the uncertainty range associated with the optical constants (Fig. 2).

Adiabatic cooling rate. We can estimate the adiabatic cooling rate that is due to atmospheric expansion under the assumption of hydrostatic equilibrium from an enhanced Jeans escape rate of N_2 and CH_4 at the exobase. The adiabatic cooling rate is given as[4]:

$$R_{adb} = -\sum_{i=1}^{2}\frac{m_i F_i}{4\pi r^2}\left(c_{p,i}\frac{\partial T}{\partial r} + \frac{GM}{r^2}\right)$$

where $i = 1$ represents N_2 and $i = 2$ represents CH_4; G is the gravitational constant; M is the mass of Pluto; r is the radial distance from Pluto's centre (as defined above);

and F_i is the number of molecules escaping per second from the global atmosphere for a gas i with mass m_i and heat capacity $c_{p,i}$. For Jeans escape processes, the escape rate for each component is approximated as[4]:

$$F = \Gamma(\lambda)\left[4\pi r^2 N\sqrt{\frac{k_B T}{2\pi m}}(1+\lambda)e^{-\lambda}\right]_{r=r_{exo}}$$

N is the number density of the molecule at exobase position r_{exo}, which is located where the mean free path of the gas molecule equals the scale height of the atmosphere. $\lambda = mgr_{exo}/k_B T$ is the Jeans parameter, where g is the gravity which varies with radial distance r. $\Gamma(\lambda)$ is the enhancement factor[4].

Timescales. The radiative relaxation timescale of gas in the bulk atmosphere is[33]:

$$\tau_{rad,g} = c_{p,g}\rho_g\left(\frac{\partial R_{net,g}}{\partial T}\right)^{-1}$$

Similarly, the radiative timescale of haze is:

$$\tau_{rad,p} = c_{p,p}\rho_p\left(\frac{\partial R_{net,p}}{\partial T}\right)^{-1}$$

The entire atmospheric radiative timescale is:

$$\tau_{rad} = (c_{p,g}\rho_g + c_{p,p}\rho_p)\left(\frac{\partial (R_{net,g}+R_{net,p})}{\partial T}\right)^{-1}$$

The thermal conduction timescale in the gas phase is approximately:

$$\tau_{cond} = \frac{c_{p,g}\rho_g H^2}{K_c}$$

where H is the scale height.

The particle sedimentation (or gravitational settling) timescale is estimated as:

$$\tau_{sed} = \frac{H}{w_{sed}}$$

where w_{sed} is the settling velocity, following equation (7) of ref. 13. For fluffy aggregated particles, the aerodynamic density needs to be corrected by taking into account porosity[38]; see ref. 13 for details. Here we use one scale height, H, as the length scale for estimating the settling timescale; ref. 13 used 1 km as the length scale.

The particles in Pluto's atmosphere are in the free-molecule regime because the mean free path (the distance between collisions) in the gas medium is more than 1,000 μm, which is much larger than the submicrometre particle size. The heat transfer between the two phases in this regime can be written on the basis of kinetic theory[39]:

$$H_{pg} = \alpha\pi r_p^2 \bar{c} k_B N_g N_p\left[\frac{1}{2}(T_p - T_g) + \int_{T_g}^{T_p}\frac{dT}{\gamma - 1}\right]$$

where α is the accommodation coefficient; r_p is the particle radius (or equivalent radius for an aggregated particle); $\bar{c}$ is the mean thermal velocity of the gas molecule; k_B is the Boltzmann constant; N_g and N_p are the number densities of the gas molecule and particle, respectively; and $\gamma = c_p/c_v$ is the adiabatic index for gas. If we set $\gamma = 1.4$ for the nitrogen-dominated atmosphere on Pluto, then the equation could be simplified as:

$$H_{pg} \approx 3\alpha\pi r_p^2 \bar{c} k_B N_g N_p (T_p - T_g)$$

Given that the temperature difference between the two phases is not large, the collisional heat-transfer timescale of a gas molecule in the particle medium can be estimated as:

$$\tau_{c,g} \approx \frac{c_{p,g}\rho_g}{3\alpha\pi r_p^2 \bar{c} k_B N_g N_p}$$

Note that for a diatomic gas molecule, the heat capacity per molecule $(c_{p,g}\rho_g/N_g)$ is about $3.5k_B$ at low temperature. Thus, approximately:

$$\tau_{c,g} \approx \frac{1}{\alpha\pi r_p^2 \bar{c} N_p}$$

If we assume that the accommodation coefficient α is unity, then $\tau_{c,g}$ is equal to the characteristic collisional timescale of a free-moving gas molecule in the particle medium.

Similarly, the collisional heat-transfer timescale of a haze particle in the gas medium can be estimated as:

$$\tau_{c,p} \approx \frac{c_{p,p}\rho_p}{3\alpha\pi r_p^2 \bar{c} k_B N_g N_p} \quad (2)$$

At the kinetic limit, we can estimate the heat capacity of the particle on the basis of the degrees of freedom:

$$\frac{\rho_p c_{p,p}}{N_p} \approx 3k_B$$

and if we assume that α is unity, then equation (2) becomes:

$$\tau_{c,p} \approx \frac{1}{\pi r_p^2 \bar{c} N_g}$$

Therefore, $\tau_{c,p}$ is roughly equal to the characteristic collisional timescale of a free-moving particle in the gas medium.

Based on the particle radius and number density profiles (Extended Data Fig. 1), the estimated timescales are shown in Fig. 3. Below 700 km, the collisional heat-transfer timescale of the gas or particle is shorter than the other heat-transfer timescales in that phase; that is, $\tau_{c,p} < \tau_{rad,p} < \tau_{sed}$, $\tau_{c,g} < \tau_{rad,g}$ and $\tau_{c,g} < \tau_{cond}$. This implies that, if there is any temperature difference between the gas and particle phases, thermal equilibrium will be quickly established by gas–particle collisions before other heat-transfer processes occur. In other words, the gas and particle should have almost the same temperature at altitudes lower than 700 km. Rigorously, the particle temperature should be slightly lower than the gas temperature so that the net collisional heat transfer is from the gas phase to the particle phase, which radiates heat away. If the accommodation coefficient is smaller than unity by a factor of two to three[40], the collisional timescales of gas and particles could be a little bit longer, but it will not alter our conclusion here. However, thermal conduction quickly dominates heat transfer in the gas phase above 700 km and maintains an isothermal atmosphere, even if particles exist in the upper atmosphere of Pluto.

Code availability. The model used here is freely available from the corresponding author upon request.

Data availability. The source data for Figs 1–4 are available online. All other data sets from this study are available from the corresponding author upon request.

31. Strobel, D. F. N_2 escape rates from Pluto's atmosphere. *Icarus* **193,** 612–619 (2008).
32. Hinson, D. P. *et al.* Radio occultation measurements of Pluto's neutral atmosphere with New Horizons. *Icarus* **290,** 96–111 (2017).
33. Zhang, X. *et al.* Radiative forcing of the stratosphere of Jupiter, Part I: atmospheric cooling rates from Voyager to Cassini. *Planet. Space Sci.* **88,** 3–25 (2013).
34. Rothman, L. S. *et al.* The HITRAN2012 molecular spectroscopic database. *J. Quant. Spectrosc. Radiat. Transf.* **130,** 4–50 (2013).
35. Häger, J., Krieger, W. & Pfab, J. Collisional deactivation of laser-excited acetylene by H_2, HBr, N_2 and CO. *J. Chem. Soc. Faraday Trans. 2.* **77,** 469–476 (1981).
36. Lavvas, P., Sander, M., Kraft, M. & Imanaka, H. Surface chemistry and particle shape: processes for the evolution of aerosols in Titan's atmosphere. *Astrophys. J.* **728,** 80 (2011).
37. Zhang, X., West, R. A., Banfield, D. & Yung, Y. L. Stratospheric aerosols on Jupiter from Cassini observations. *Icarus* **226,** 159–171 (2013); erratum **266,** 433–434 (2016).
38. Lavvas, P., Yelle, R. V. & Griffith, C. A. Titan's vertical aerosol structure at the Huygens landing site: constraints on particle size, density, charge, and refractive index. *Icarus* **210,** 832–842 (2010).
39. Filippov, A. V. & Rosner, D. E. Energy transfer between an aerosol particle and gas at high temperature ratios in the Knudsen transition regime. *Int. J. Heat Mass Transfer* **43,** 127–138 (2000).
40. Burke, J. R. & Hollenbach, D. J. The gas-grain interaction in the interstellar medium—thermal accommodation and trapping. *Astrophys. J.* **265,** 223–234 (1983).

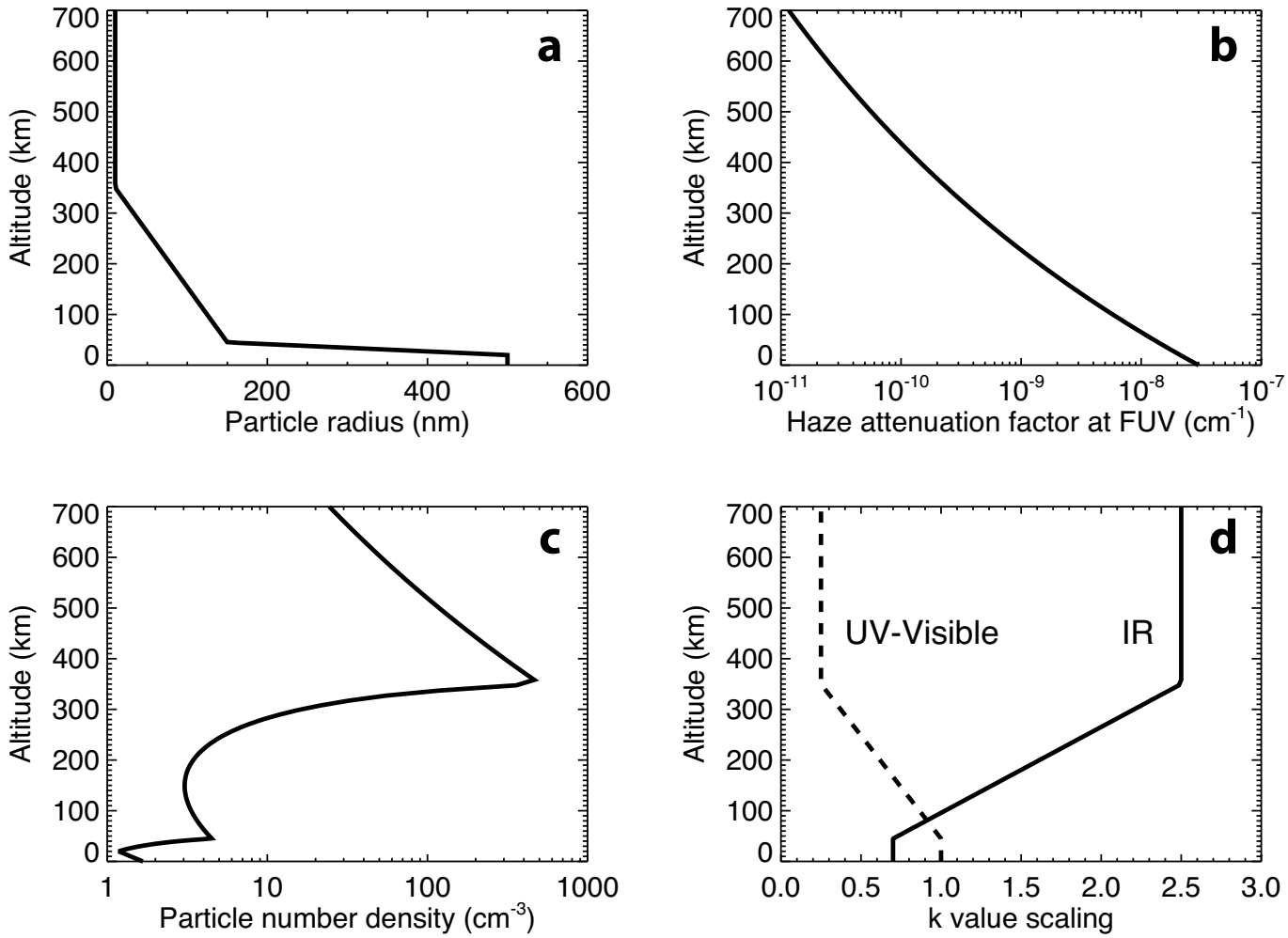

Extended Data Figure 1 | Properties of haze in Pluto's atmosphere as a function of altitude. Vertical distributions of: **a**, the mean particle size; **b**, the observed haze attenuation factor at the Alice far-ultraviolet (FUV) channel; **c**, particle number density; and **d**, scaling factors applied to the haze *k* values in our balanced model.

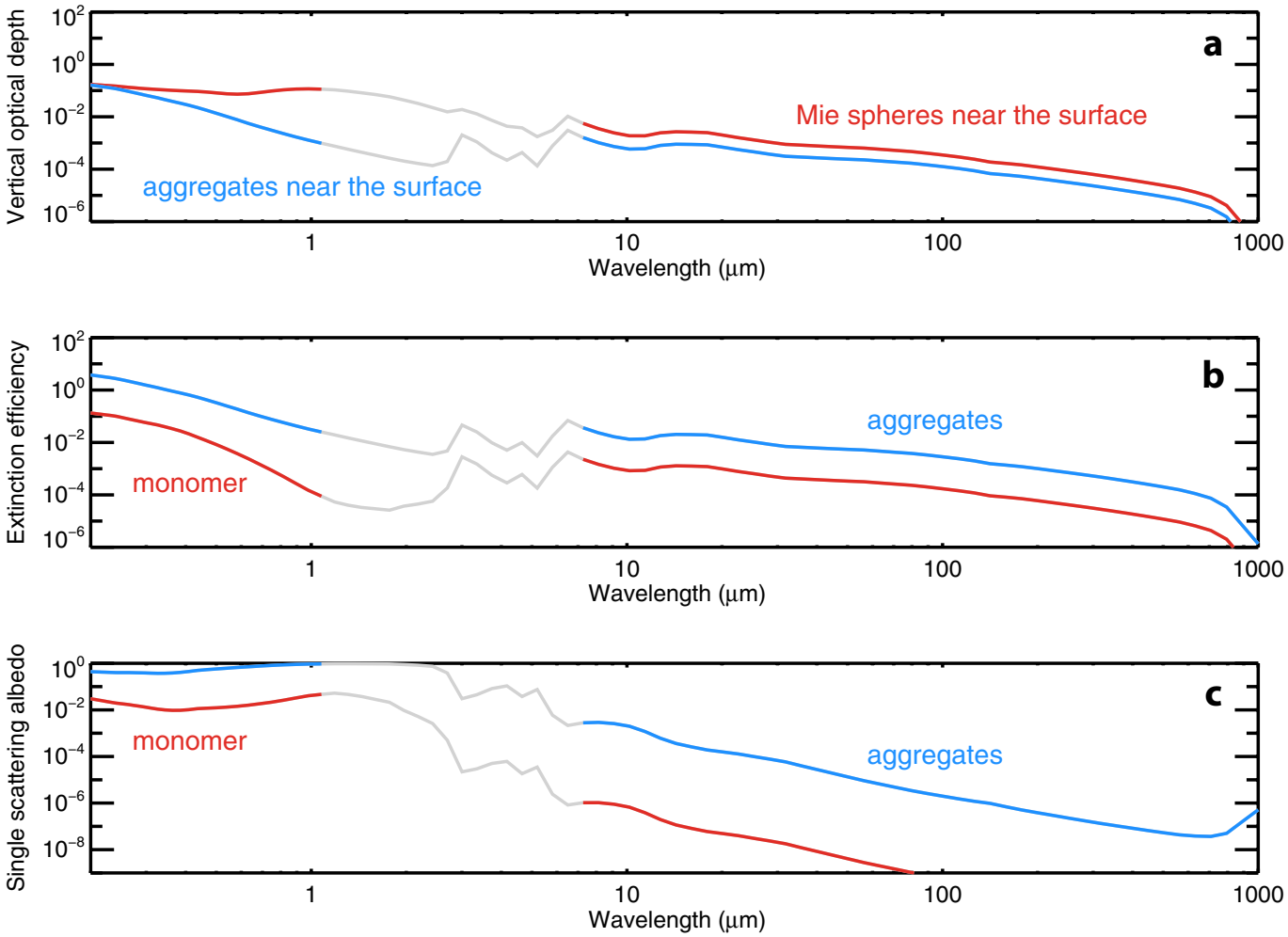

Extended Data Figure 2 | Optical properties of haze in Pluto's atmosphere as a function of wavelength. a, Total vertical optical depths of haze for two cases: if the particles in the near-surface layers are Mie spheres, or if they are fractal aggregates. **b**, Extinction efficiencies for a 10-nm monomer particle and an aggregated particle composed of 10-nm monomers with a volume-equivalent radius of 0.15 μm (ref. 3). Extinction efficiency for the aggregates is defined as the calculated total extinction cross-section divided by the cross-section of equal-volume spheres[22]. **c**, Single scattering albedos as a function of wavelength. The contribution of the spectral region from 1 μm to 7 μm (grey lines) to the haze heating rate is less than 1% and is omitted here.

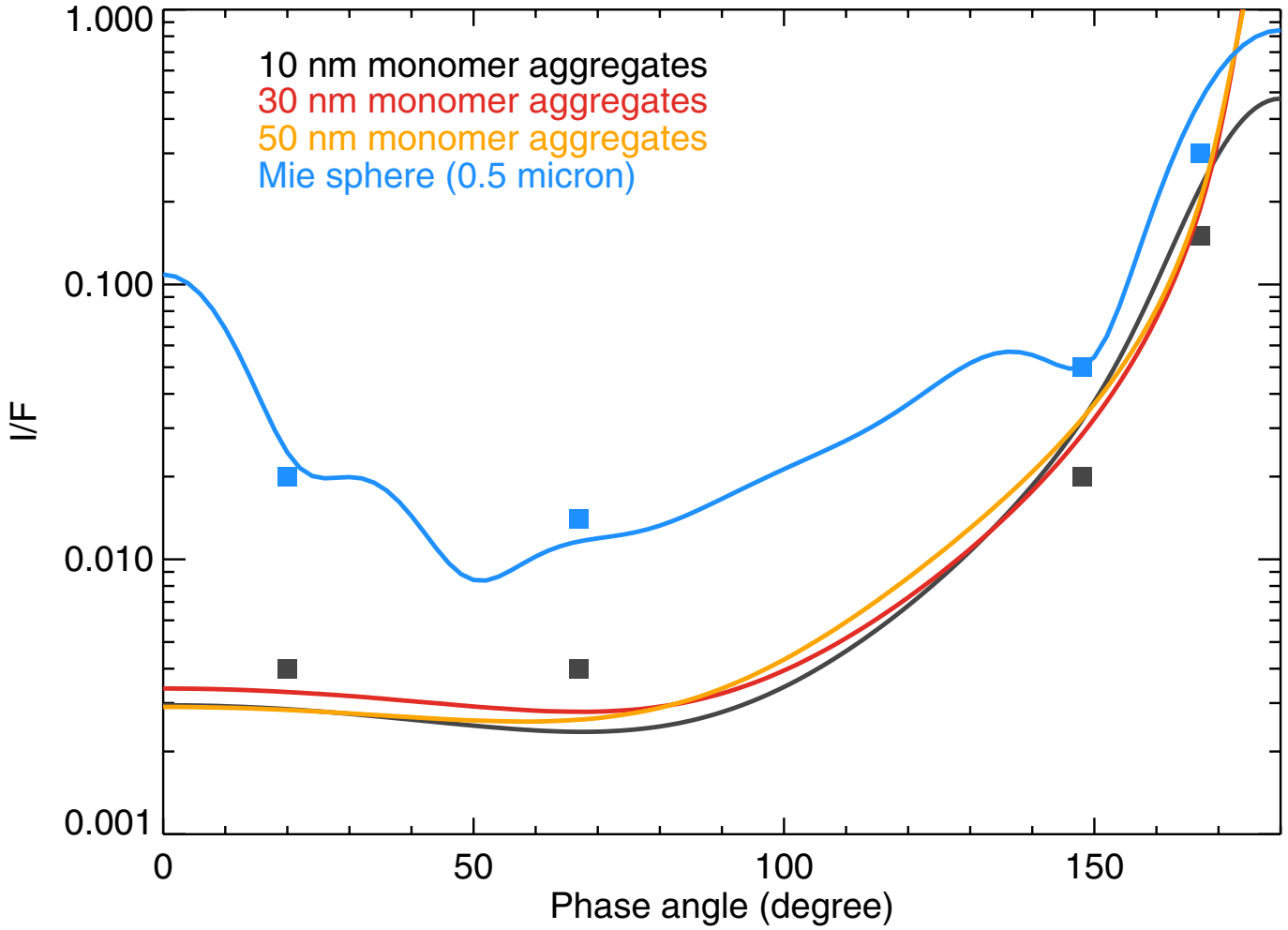

Extended Data Figure 3 | Reflectivity *I*/*F* values as a function of phase angle. LORRI observations at an altitude of 45 km (black) and near the surface (blue) are shown with squares[3]. Simulated phase functions from multiple solutions of aggregates (composed of 10-nm monomers, 30-nm monomers or 50-nm monomers) are scaled to fit the observations.

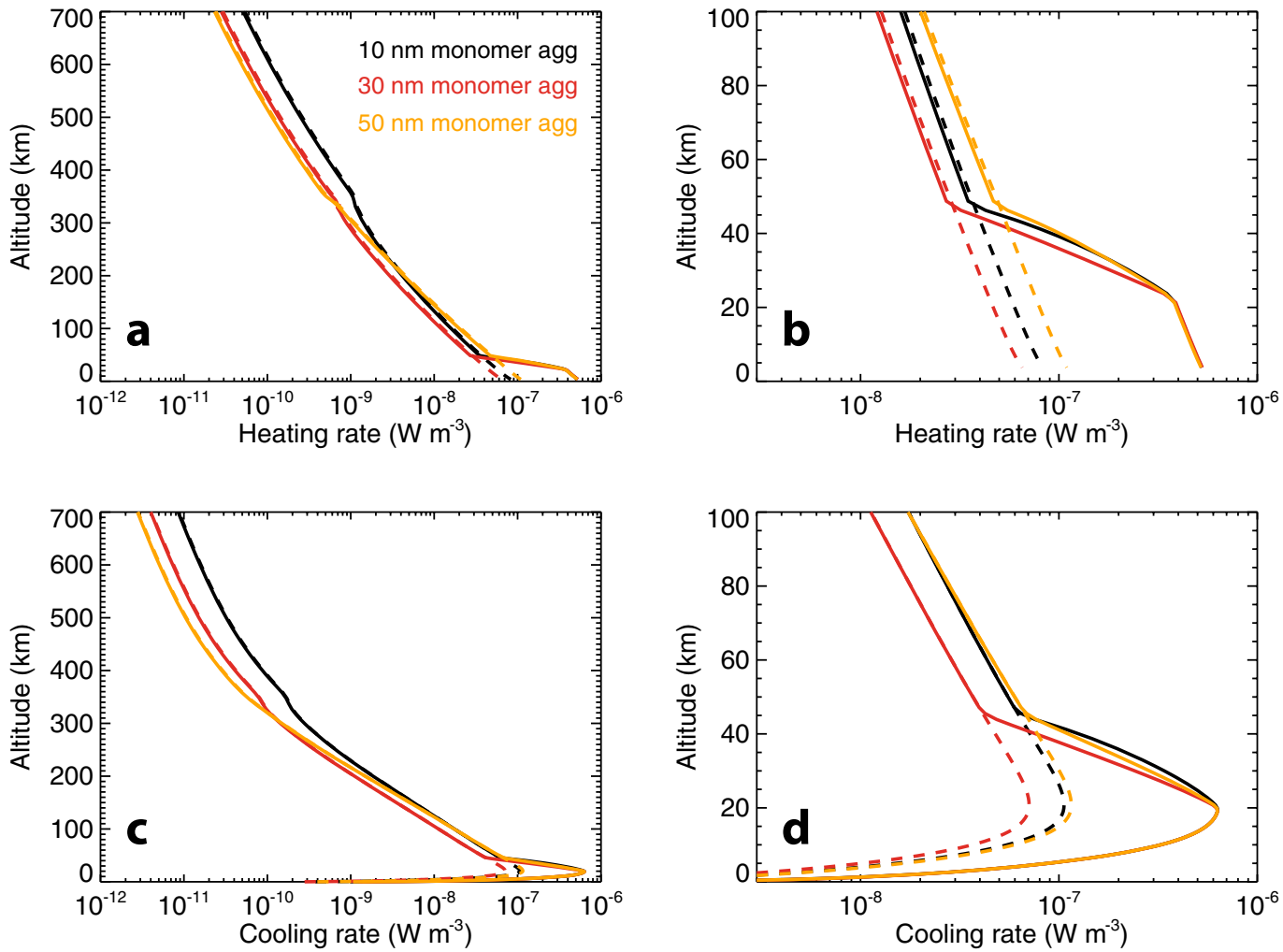

Extended Data Figure 4 | Sensitivity study of haze heating and cooling rates. a, **b**, Modelled heating rates. **c**, **d**, Modelled cooling rates. Solid lines represent the results obtained if the near-surface haze layers are composed of Mie-sphere particles with radii of 0.5 μm. Dashed lines show the results obtained if the near-surface particles are instead aggregates identical to those at 45 km (consistent with Extended Data Fig. 3). **b**, **d**, Zoomed-in versions of **a** and **c**, respectively, for the lower 100-km region.